Chemical Engineering Journal 265 (2015) 228–238

Contents lists available at ScienceDirect

Chemical Engineering Journal

journal homepage: www.elsevier.com/locate/cej

A simple hydrothermal approach to modify palygorskite for high-efficient adsorption of Methylene blue and Cu(II) ions

Wenbo Wang [a,c], Guangyan Tian [a,b], Zhifang Zhang [a,b], Aiqin Wang [a,c,*]

[a] Center of Eco-materials and Green Chemistry, Lanzhou Institute of Chemical Physics, Chinese Academy of Sciences, Lanzhou 730000, PR China
[b] University of the Chinese Academy of Sciences, Beijing 100049, PR China
[c] R&D Center of Xuyi Attapulgite Applied Technology, Lanzhou Institute of Chemical Physics, Chinese Academy of Sciences, Xuyi 211700, PR China

HIGHLIGHTS

- Hybrid silicate adsorbents were prepared by one-step hydrothermal process.
- Magnesium silicate was formed and form a uniform composite structure with PAL.
- The inert quartz impurity was transformed as active amorphous magnesium silicate.
- The adsorbent shows superior adsorption capacity for Methylene blue and Cu(II) ions.
- This provides a new approach to fabricate eco-friendly high-performance adsorbent.

GRAPHICAL ABSTRACT

ARTICLE INFO

Article history:
Received 1 November 2014
Received in revised form 27 November 2014
Accepted 28 November 2014
Available online 18 December 2014

Keywords:
Palygorskite
Magnesium silicate
Methylene blue
Heavy metal
Adsorption

ABSTRACT

Silicate materials have been frequently used as stable, low-cost and efficient adsorbents for the removal of dyes and heavy metal ions from aqueous solution. Herein, at the aim of designing new adsorbent with higher adsorption capacity, natural palygorskite (PAL) was modified *via* a one-step hydrothermal process by introducing sodium silicate and magnesium salts. The effect of Si/Mg dosage ratio on the structure and physico-chemical features of the adsorbent was investigated, and its adsorption capability for Methylene blue (MB) and Cu(II) ions was intensively evaluated. It was found that Si/Mg dosage ratio is the key to control the adsorption properties of the adsorbent. The active magnesium silicate could be formed around PAL at the moderate Si/Mg dosage ratio, and even the undesirable quartz impurities without adsorption activity in the natural PAL minerals may transform as amorphous magnesium silicate with higher adsorption activity in this process. The adsorbent shows greater BET specific surface areas (407.3 m^2/g), ideal surface charge distribution and superior adsorption capacity to MB and Cu(II) ions, with the maximum adsorption capacity of 527.22 mg/g for MB and 210.64 mg/g for Cu(II) ions at the Si/Mg dosage ratio of 2:1. The MB molecules and Cu(II) ion could be almost completely removed from 100 mg/L of MB solution and 25 mg/L of Cu(II) solution by the adsorbent, respectively, which is far away higher than that of raw PAL. The electrostatic attraction, ion exchange and chemical association of $-Si-O^-$ groups contribute to the enhanced adsorption for MB or Cu(II) ions.

* Corresponding author. Addresses: Center of Eco-materials and Green Chemistry, Lanzhou Institute of Chemical Physics, Chinese Academy of Sciences, Lanzhou 730000, PR China and R&D Center of Xuyi Attapulgite Applied Technology, Lanzhou Institute of Chemical Physics, Chinese Academy of Sciences, Xuyi 211700, PR China. Tel.: +86 931 4968118; fax: +86 9318277088.
E-mail address: aqwang@licp.cas.cn (A. Wang).

http://dx.doi.org/10.1016/j.cej.2014.11.135
1385-8947/

1. Introduction

Large amounts of toxic weakly biodegradable dyes and heavy metal ions discharged from the textile, rubber, plastic and electroplate industries arouse a detrimental risk to human health, living organisms and ecosystem, and so their removal from wastewater by an ecological and efficient method becomes urgent and the correlational researches have attracted worldwide concerns [1–3]. Among numerous methods, adsorption has been especially concerned as an economic, effective method to remove pollutants because of its incomparable advantages, e.g., low cost, ease of operation, high resistance towards toxic chemical compounds in water, and the flexibility of structure design of adsorbent [4–9]. Undoubtedly, adsorbents are the core of adsorption technique, and the desirable adsorbents would be highly efficient, stable, low-cost, non-toxic and environmentally compatible.

Silicates, as the materials of "greening 21st century material world" [10], have found extensive applications as naturally available low-cost adsorbents [11–13]. Palygorskite (PAL) is a special one-dimensional nanorod-like silicate with a 2:1 ribbon-layer structure composed of two continuous tetrahedron sheets and one discontinuous octahedron sheet [14]. The abundant resource, nanorod-like morphology, higher stability and plentiful nanoporous feature of PAL endow it with inherent advantages to be developed as a variety of promising adsorbents for removing dyes [5,9,15], heavy-metals [4,7,16,17] and other organic pollutants [8,18]. It could be predictable that the PAL-based adsorbents will be stable, safe, low cost, and non-toxic. More importantly, such adsorbents do not induce the risk of secondary pollution (i.e., the usage of some organic adsorbents may induce the increase of COD in water). However, the adsorption capability of natural PAL is usually limited, which must be moderately modified to reach a satisfactory adsorption capability before using as an adsorbent.

The modification of PAL by various physical or chemical methods has been engaged considerable efforts in both academic and industrial areas. The physical grinding treatment of PAL may enhance its adsorption capacity for Methylene blue (MB) by disaggregating the crystal bundles and exposing more surface groups [15]. The thermal treatment may remove the water molecules in the tunnel of PAL and break the Si–O–M bonds to enhance the adsorption capacity for MB [19]. The moderate acid activation may create "cavity sites" in PAL and thus enhance the adsorption capacity for Cu(II) [19]. The organification modification of PAL may enhance its adsorption for anionic dye by altering surface charges [20]. It could be summarized from previous researches that the main principle of enhancing the adsorption capacity is that the inert Si–O–Si or Si–O–M bonds in the crystal were broken, and many active –Si–O^- groups or exchangeable cations could be generated, which may increase the exchange and association capability of PAL with absorbates. That is to say, to adjust the crystal structure and surface feature of PAL are extremely important to design and fabricate new adsorbents with excellent adsorption properties.

The hybrid methods, including organic–inorganic and inorganic–inorganic hybrids, are commonly recognized as a very effective strategy to produce new materials superior to either of the components. The organic–inorganic hybrid method has been frequently employed to fabricate the adsorbents for wastewater treatment [8,9]. However, the usage of organic matter in such material always cannot get rid of the risk that the organic component may be leaked to the water and induced the secondary pollution. Thus, the hybrid silicate materials derived from natural clay and synthetic silicate will be safer and potential because they not only combine the advantages of each component, but also exhibit some desirable features, e.g., excellent stability, non-toxicity and compatibility.

Magnesium silicates have unique structure, ion exchange and adsorption properties, and are developed as the ideal absorbents in many fields, such as water purity [21]. In particular, the cation-exchange and negatively charged features of the hybrid material containing magnesium silicate allow it to be applied for the separation and recovery of toxic heavy metal ions or dyes from contaminated water [21,22]. Hydrothermal treatment may induce the evident enhancement of performance by slightly changing the crystal structure [23]. It is possible to create new adsorption sites and enhance adsorption properties by the hydrothermal modification of PAL with silicate and magnesium salts, but rare research concerns on this subject.

Herein, we report a simple hydrothermal approach to modify PAL with sodium silicate and magnesium salts for preparing an adsorbent with excellent adsorption performance and eco-friendly characteristic. The morphology, structure and composition of the obtained adsorbents were fully investigated by Fourier transform infrared spectra (FTIR), scanning electronic microscope (SEM), transmission electronic microscope (TEM), X-ray diffraction (XRD) and X-ray fluorescence (XRF) techniques. In addition, the adsorption properties of the adsorbent were investigated using MB and Cu(II) ions as the model pollutants.

2. Experimental

2.1. Materials

Palygorskite (PAL) clay mineral was produced from Gaojiawa Mine located at Xuyi county of Jiangsu province, China, which was pretreated by rolling for one times. Methylene blue (MB, A.R. grade) and copper sulfate pentahydrate ($CuSO_4{\cdot}5H_2O$) was purchased from Sinopharm Chemical Reagent Co., Ltd (Shanghai, China). Magnesium sulfate heptahydrate ($MgSO_4{\cdot}7H_2O$, A.R. grade), sodium metasilicate nonahydrate ($NaSiO_3{\cdot}9H_2O$, A.R. grade) and Neocuproine Hemihydrate (A.R. grade) were purchased from Aladdin Reagent Inc. (Shanghai, China). All other reagents are of analytical grade and all solution was prepared with deionized water.

2.2. Modification of PAL with silicon- and magnesium salts

Pretreated PAL powder (1.8 g) was dispersed in 30 mL of aqueous solution containing $Na_2SiO_3{\cdot}9H_2O$ (7.8 g) to form a homogeneous suspension, and then 20 mL of aqueous solution of $MgSO_4{\cdot}7H_2O$ (the mass was controlled according the Si/Mg dosage ratio of 1:0, 3:1, 2:1, 1:1, 1:2, and 1:3) was added dropwise to the resultant suspension under continuous stirring. The white solid was gradually formed. Finally, the mixture was transferred into a Teflon Tank, sealed and reacted at 180 °C for 24 h. The reaction parameters including solid/liquid ratio, temperature and reaction time were optimized and discussed in the Supporting materials. In this paper, effect of the Si/Mg dosage ratio was mainly studied based on the optimal reaction parameters (reaction temperature, 180 °C; reaction time, 24 h; solid/liquid ratio, 1:33).

2.3. Adsorption experiments

Batch adsorption experiments were performed by contacting 0.025 g of adsorbents with 25 mL of MB (or Cu(II) ion) solution in a thermostatic shaker (THZ-98A) at 120 rpm and 30 °C to reach adsorption equilibrium. The solution was rapidly separated from the adsorbent by a 0.22 μm filter. The concentration of MB solution before and after adsorption was analyzed by determining the absorbance of the solution at the maximum wavelength of 664 nm using a UV–vis spectroscopy. The concentration of Cu(II) solution before and after adsorption was determined by a ICP

plasma emission spectrometer (iACP 6300, Thermo Fisher, USA). The adsorption capacity of the adsorbents for MB (or Cu(II) ions) can be calculated by the following Eq. (1):

$$q = (C_0 - C_e)\ V/m \quad (1)$$

where q is the amount of MB (or Cu(II) ion) adsorbed by per unit mass of adsorbent at time t (q_t, mg/g) or at equilibrium (q_e, mg/g), V is the volume of MB (or Cu(II) ions) solution used (mL), C_0 and C_e are the initial and final concentration of MB (or Cu(II) ions) solution (mg/L) and m is the mass of adsorbent (mg). In current work, a set of MB solutions with the concentrations of 100–1500 mg/L (pH 7) were adopted to investigate the adsorption isotherms for MB. A set of Cu(II) solutions with the concentrations of 50–1200 mg/L (pH 5) were adopted to investigate the adsorption isotherms for Cu(II) ions. The MB solution with initial concentration of 500 mg/L and the Cu(II) solution with initial concentration of 200 mg/L were used to evaluate the effect of pH values (from 2 to 7 for MB and 2 to 5 for Cu(II)) on the adsorption.

The adsorption kinetics was determined according to the following procedure: 25 mL of the MB solution (pH 7; initial concentrations, 100 and 800 mg/L) or Cu(II) solution (pH 5; initial concentrations, 50 and 200 mg/L, respectively) was fully contacted with 25 mg of adsorbent, and then the solution was separated by filtering at different intervals (5–120 min for MB and 5–180 min for Cu(II)). The adsorption amount of the adsorbent for MB (or Cu(II)) could be determined and calculated by the method described above. All experiments were parallel carried out for three times, and the averages are reported.

2.4. Characterizations

The surface morphology of samples was observed using a field emission scanning electron microscope (FESEM, JSM-6701F, JEOL, Ltd.) after the samples were fixed on copper stubs and coated with gold film. TEM image was observed using a JEM-1200 EX/S transmission electron microscope (TEM) (JEOL, Tokyo, Japan). The XRD patterns were performed on an X'Pert PRO diffractometer equipped with a Cu Kα radiation source (40 kV, 40 mA). FTIR spectra were recorded on a Thermo Nicolet NEXUS TM spectrophotometer in the range of 4000–400 cm^{-1} using a KBr platelet. The specific surface area was measured on ASAP 2010 analyzer (Micromeritics, USA) at 77 K by determining the N_2 adsorption–desorption isotherms. The values of specific surface area (S_{BET}) were calculated by the BET equation. The total pore volumes (V_{total}) were obtained from the volume of liquid N_2 held at the relative pressure $P/P_0 = 0.95$. The micropore volume (V_{micro}) was estimated by the t-plot method. The chemical composition was determined using a Minipal 4 X-ray fluorescence spectrometer (PANalytical, Netherland). Zeta potentials were measured on a Malvern Zetasizer Nano system with irradiation from a 633 nm He–Ne laser (ZEN3600). The aqueous suspension (0.5%, w/v) for measurement was prepared by dispersing the samples into de-ionized water using a high-speed stirring at 10,000 rpm.

3. Results and discussion

3.1. FTIR spectra analysis

The FTIR spectra of PAL and the adsorbents are shown in Fig. 1. As can be seen, the absorbance band of PAL at 3548 cm^{-1} (stretching vibration of (Fe/Mg) O–H and (Al/Mg) O–H) disappeared and the band at 1196 cm^{-1} (stretching vibration of Si–O–Si groups connected two reverse tetrahedrons) become weaker (Fig. 1b) after being modified with Na_2SiO_3 (Si/Mg dosage ratio is 1:0), which implies that the ribbon-layer structure of PAL crystal was changed during hydrothermal reaction in the presence of Na_2SiO_3 [24]. Simultaneously, the band of carbonate at 1455 cm^{-1} (ascribed to dolomite) (Fig. 4a) becomes weaker, and shifts to 1398 cm^{-1} (ascribed to calcite) (Fig. 1b) after reaction, indicating that the dolomite-type carbonates participate in the reaction. The new band appears at about 3680 cm^{-1} (the Mg_3O–H stretching vibration) when the Na_2SiO_3 and Mg^{2+} ions were simultaneously introduced, and the same band at 3679 cm^{-1} also appeared in the FTIR spectrum of neat magnesium silicate (Fig. S1, see Supporting materials), which confirms the formation of magnesium silicate complex. At the same time, the absorbance band of SiO_2 at 793 cm^{-1} was clearly weakened after reaction, and almost disappeared at the Si/Mg dosage ratio of 2:1. It means that the inert SiO_2 impurity that is associated with PAL reacted with Mg^{2+} ions to form the magnesium silicate with certain adsorption activity. The H–O–H bending vibration band at 1653 cm^{-1}, ascribed to the adsorbed water, zeolite water and coordination water in PAL, shifts to 1640 cm^{-1} (Si/Mg dosage ratio, 2:1), 1639 cm^{-1} (Si/Mg dosage ratio, 1:1), 1640 cm^{-1} (Si/Mg dosage ratio, 1:2), 1642 cm^{-1} (Si/Mg dosage ratio, 1:3), which reveals that the existence of more Mg^{2+} ions in the adsorbent may be helpful to intensify the interaction of water molecules with the PAL.

3.2. SEM and TEM analysis

Fig. 2 shows the typical SEM and TEM images of the adsorbents prepared at different Si/Mg dosage ratios. It is obvious that the number of PAL nanorods reduced and the surface of rod becomes coarse after hydrothermal reaction with Na_2SiO_3 (Fig. 2a). Many longer rods are broken as short rods or particles, and some amorphous or plate-shape matters could be observed. This reveals that ribbon-layer structure of PAL may be broken and transformed as amorphous matters in the alkali solution of Na_2SiO_3 [25]. When the Si/Mg dosage ratio increases to 2:1, the breakage of rods is slightly alleviated, and many amorphous matters (as confirmed by XRD analysis) are formed around rods to form a hybrid material, which may be due to the formation of magnesium silicate after introducing Mg^{2+} ions (Fig. 1b and f). With further increasing the Mg/Si dosage ratio to 1:1, the PAL nanorods have no obvious change, and they are embedded within the plate-shape or amorphous matters (Fig. 1c and e). This reveals that the increase of Mg^{2+} dosage is favorable to restrain the breakage of PAL nanorods, and the amorphous magnesium silicate can be *in situ* formed. The fragment of amorphous matters obviously increased with further increasing the Mg/Si dosage ratio to 2:1. The TEM image also shows the coexistence of sheet-shape silicate with the PAL rods. At the ratio of 1:1, the PAL rods are dominant; while the sheet-shape crystals are dominant at the Si/Mg dosage ratio of 2:1. The coexistence of sheets and rods may be favorable to the adsorption properties.

3.3. XRD analysis

The XRD analyses also give the similar results with SEM and TEM observation for the change of microstructure. As can be seen from Fig. 3, after modified with Na_2SiO_3, the (1 1 0) diffraction peak at $2\theta = 8.50°$ ($d = 1.0390$ nm) obviously weakens and shifts to $2\theta = 8.36°$ ($d = 1.0564$ nm) [26]. Meanwhile, the (2 0 0) diffraction peak at $2\theta = 13.86°$ and the (2 4 0) diffraction peak at $2\theta = 24.38°$ disappeared. The new peaks, ascribed to the diffraction peak of analcite, appear at $2\theta = 16.04°$ and 26.19°. This reveals that the ribbon-layer structure of PAL was damaged to form a new crystal phase (Fig. 3b), which is consistent with the SEM and TEM results. With increasing the Si/Mg dosage ratio to 3:1 and 2:1, the (1 1 0) diffraction peak of PAL, the characteristic peak of quartz ($2\theta = 26.87°$) and the characteristic peak of dolomite ($2\theta = 31.16°$)

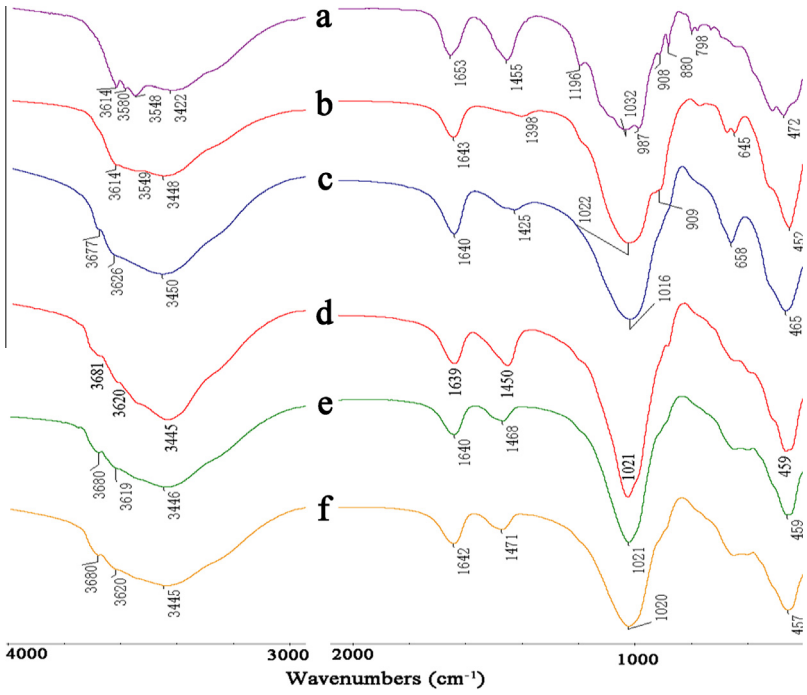

Fig. 1. FTIR spectra of raw PAL (a) and the adsorbents with different Si/Mg dosage ratio of (b) 1:0, (c) 2:1, (d) 1:1, (e) 1:2, (f) 1:3.

disappeared; while the intensity of diffraction peak of calcite ($2\theta = 29.59°$) slightly increased. Besides, no other peak of new crystal phase could be observed. This reveals that most of the PAL crystal was transformed as an amorphous state, and dolomite ($CaMg(CO_3)_2$) participates in the reaction by transforming as calcite ($CaCO_3$). The disappearance of peak of quartz means that the inert SiO_2 impurity may also be transferred as active amorphous magnetism silicate with better adsorption activity. This result is encouraging because it may transform un-desirable quartz impurity to a desirable adsorption component (Fig. 3c and d).

The XRF results (Fig. 4) may confirm the formation of magnesium silicate during hydrothermal reaction (the Mg content was clearly increased), but the diffraction peaks of $Mg_3Si_2O_5(OH)_4$ (JCPDS No. 52-1562) are absent in the diffraction pattern of the adsorbent, which may be related to the imperfect crystallinity degree of the adsorbent. With increasing the dosage of Mg^{2+} ions, the (1 1 0) peak was observed again, but its intensity is obviously lower than that of raw PAL, which implies the crystallinity of PAL decreased. Simultaneously, the peak of quartz appeared again, but the intensity is obviously lower than that of raw PAL (Fig. 3e–g). This means that the excessive Mg^{2+} ion is adverse to the transformation reaction of PAL and quartz. Meanwhile, the new crystal phase of magnesium silicate was observed at $2\theta = 25.52°$ for the sample with Si/Mg dosage ratio of 1:2 and 1:3, indicating that the enough Mg^{2+} ions in the reaction system is favorable to increase the crystallinity of magnesium silicate.

3.4. XRF analysis

As shown in Fig. 4, the MgO content was slightly decreased after treated PAL with aqueous solution of Na_2SiO_3, which confirms that the Si–O–Mg bonds may be broken and the partial Mg^{2+} ions was leached (Fig. 4a). With increasing the dosage of Mg^{2+} ions (the dosage of SiO_3^{2-} is fixed), the MgO content was sharply increased, which reaches 15.61%, 18.75%, 28.97%, 28.66% and 28.48% for the samples with Si/Mg dosage ratio of 3:1, 2:1, 1:1, 1:2 and 1:3, respectively. The MgO content does not increase further with increasing the Mg^{2+} dosage (i.e., the Si/Mg dosage ratio is 1:2 and 1:3). This confirms that the Mg^{2+} ions reacted with Na_2SiO_3 to form magnetism silicate. The content of SiO_2 and Al_2O_3 decreased with increasing the dosage of Mg^{2+}. The Al_2O_3 in the adsorbent is mainly derived from PAL. With increasing the dosage of Mg^{2+} ions, the ratio of the magnesium silicate in the adsorbent increased, and so the content of Al_2O_3 certainly decreases.

3.5. N_2 adsorption–desorption isotherm

The N_2 adsorption–desorption isotherms of the adsorbents were determined at 77 K and are shown in Fig. 5. As described previously, the isotherm of raw PAL can be classified as Type-II according to IUPAC classification with the H3-type hysteresis [27,28]. The modified PAL with only Na_2SiO_3 (without adding Mg^{2+} ions) also shows a Type-II isotherm with H3 hysteresis. The adsorption amount of N_2 for the modified PAL gradually increases with increasing the relative pressure in the region of $P/P_0 \leqslant 0.40$, and the adsorption and desorption curves are overlapped in this region, with the N_2 adsorption amount of 39.8 cm^3/g, which reveals the presence of little micropores and monolayer adsorption. The adsorption amount of N_2 was sharply increased at $P/P_0 > 0.4$ due to the capillary of N_2 in the mesopores (and/or macropores) and its multilayer adsorption on the mesopores and macropores, and H3-type hysteresis at relatively higher pressure was observed, indicating the existence of mesopores and/or macropores [27,29], and the pores in the adsorbents are narrow slit-like pores or aggregates of plate-like particles [30].

After introducing Mg^{2+} ions during reaction, the shape of the isotherm is different from that of raw PAL. The hysteresis loops at the relative pressure higher than 0.4 becomes wide for the adsorbent with Si/Mg dosage ratio of 2:1, but become narrow for 1:1 and 1:2, indicating that the adsorbents have different pore size distribution or pore morphology. The specific surface area of the adsorbent with Si/Mg dosage ratio of 2:1 is much higher than that of raw PAL.

The pore size distributions (PSD) of mesopores in the adsorbents were calculated by BJH (Barret–Joyner–Halenda) method from the adsorption branches (Fig. 6). The resultant pore size dis-

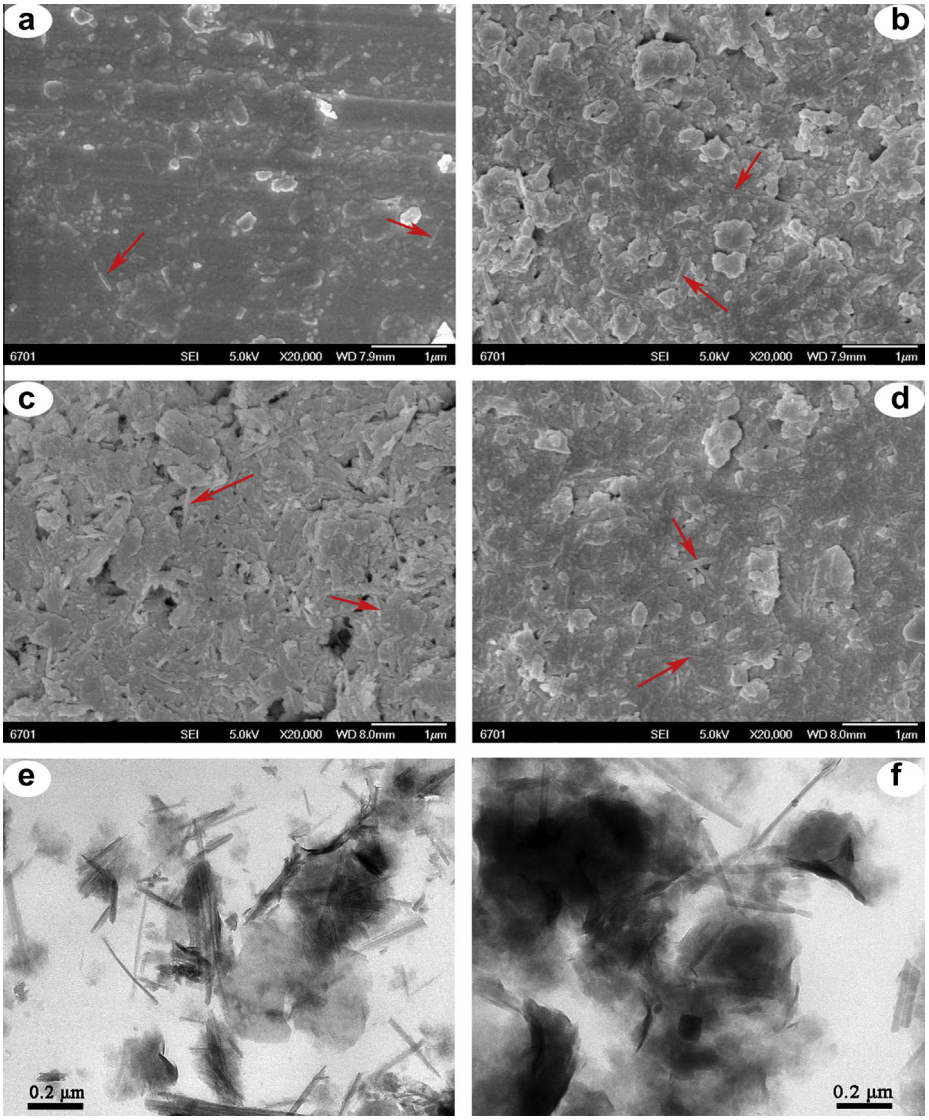

Fig. 2. The SEM (a–d) and TEM (e, f) images of the adsorbents with Si/Mg dosage ratio of (a) 1:0, (b)2:1, (c) 1:1, (d) 1:2, (e) 1:1 and (f) 2:1.

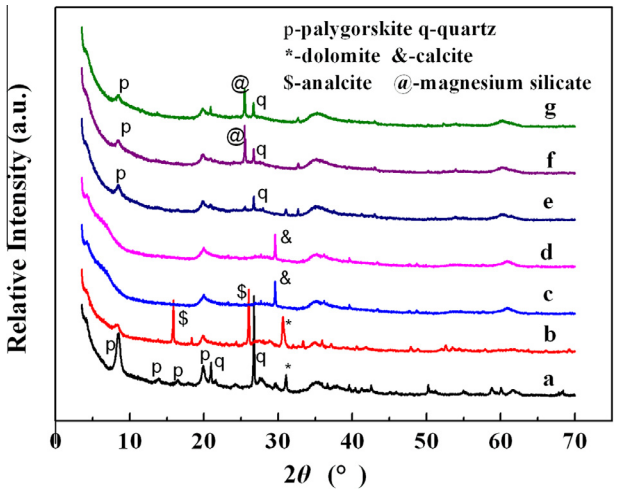

Fig. 3. XRD patterns of raw PAL (a) and modified PAL with different Si/Mg ratio of (b) 1:0, (c) 3:1, (d) 2:1, (e) 1:1, (f) 1:2, (g) 1:3.

tribution curve of the modified PAL with Na_2SiO_3 from the BJH method (Fig. 6) mainly exhibits two peaks: one is at 3.42 nm, which can be assigned to the close-packed PAL nanoparticles; another is at about 11.18 nm, which can be attributed to the aggregation of PAL particles [31]. The first peak was shifted to 3.65 nm, 3.47 nm and 3.41 nm for the adsorbents with Si/Mg dosage ratio of 2:1, 1:1 and 1:2, respectively. The total pore volume at this pore size increased, which reaches the maximum value at the Si/Mg dosage ratio of 1:2. The peak at 11.18 nm almost disappeared for samples with Si/Mg dosage ratio of 2:1, 1:1 and 1:2, which implies that the adsorbent has narrow pore-size distribution.

3.6. Zeta potentials

The variation of Zeta potential can usually reflect the change of surface groups of clay. As shown in Fig. 7a, the Zeta potential of raw PAL is −20 mV, which clearly decreases to −52.5 mV after modified with Na_2SiO_3. This confirms that the Si–OH was transferred as $Si–O^-Na^+$ and some Si–O–Si bonds may be broken to form $–Si–O^-$ groups under the alkali attack in hydrothermal process [25], which is favorable to decrease the surface potential of PAL. With increasing the dosage of Mg^{2+} ions, the Zeta potential gradually increases, and is almost equal to the value of raw PAL at the Si/Mg dosage ratio of 1:1. With further increasing the dosage of Mg^{2+}, the Zeta potential tends to be constant, indicating that the further addition of Mg^{2+} ions does not clearly affect the surface charges. By

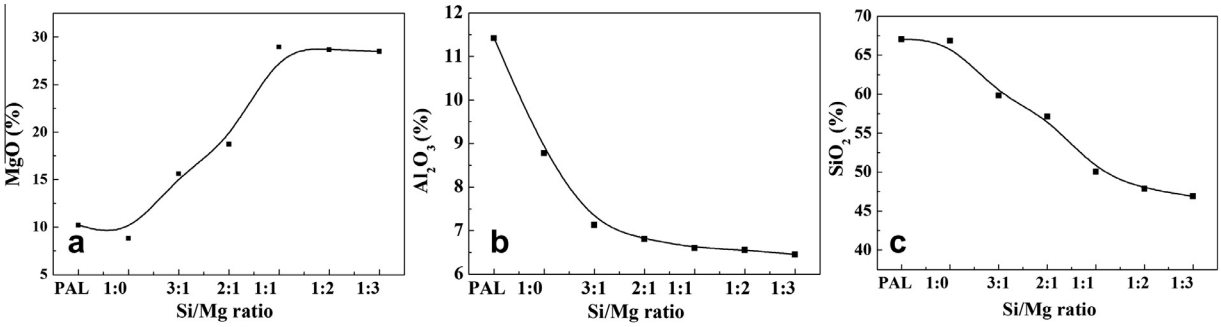

Fig. 4. Variation of chemical composition of the adsorbents with different Si/Mg dosage ratio.

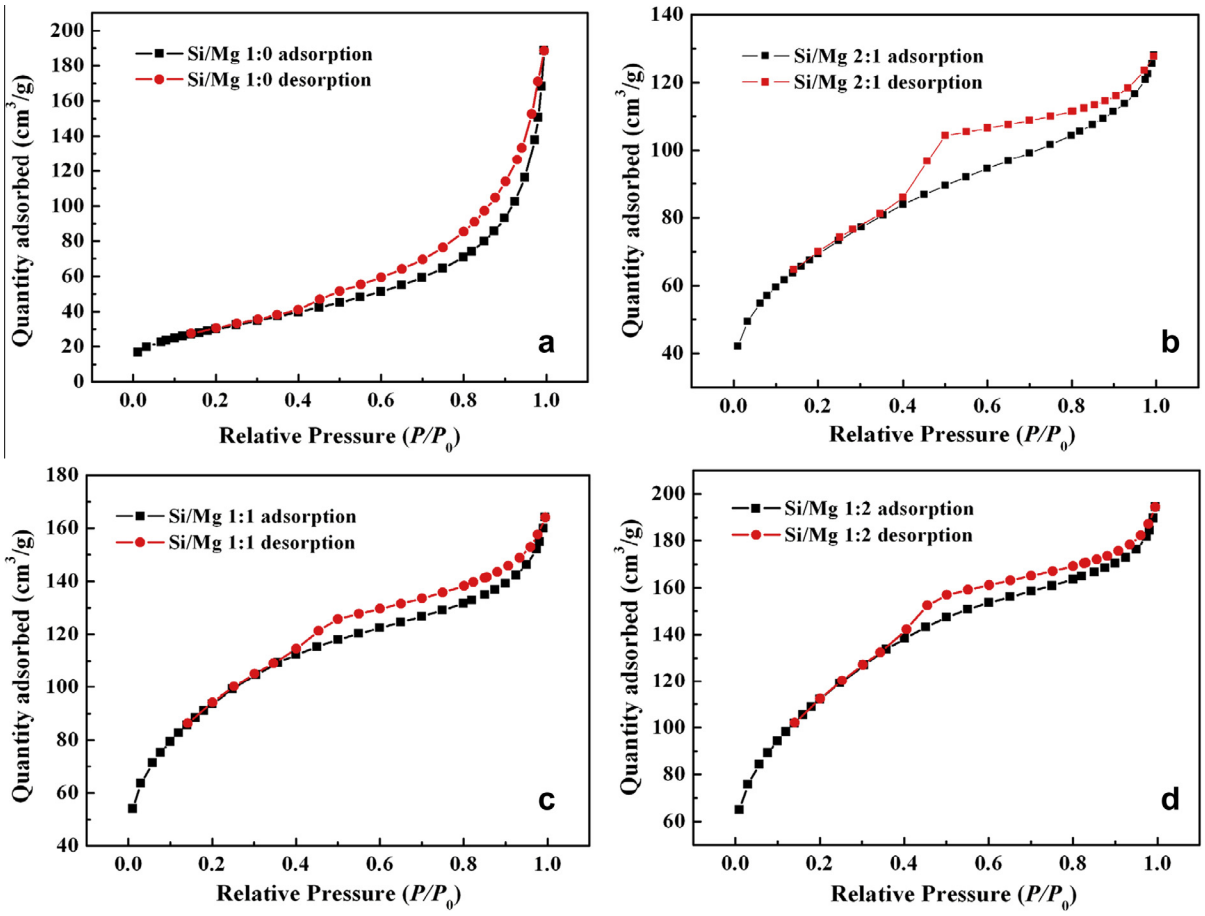

Fig. 5. N_2 adsorption–desorption isotherms of the adsorbents.

correlating the Zeta potentials with the initial pH values (Fig. 7b), it can be found that the higher pH corresponds to a lower Zeta potential, and the alkali condition is essential to make the surface charges of the adsorbent become more negative.

3.7. Adsorption isotherms for MB and Cu(II) ions

Fig. 8 shows the variation of adsorption capacity of raw PAL and the adsorbents for MB *vs* the initial concentrations. As can be seen, the adsorption capacities sharply increased with increasing the initial concentration of MB solution, and then tend to equilibrium. This indicates that the increase of initial dye concentration contributes to enhance the driving force at the solid–liquid interface (ion exchange, electrostatic attraction and chemical association) until the adsorption sites were saturated. In order to well describe the adsorption behaviors (i.e., the extent of adsorption and relevant mechanism) [32], the experimental data was fitted with the Freundlich (Eq. (2)) [33] and Langmuir (Eq. (3)) [34] isotherm models:

$$\log q_e = \log K + (1/n) \log C_e \quad (2)$$

$$C_e/q_e = 1/(q_m b) + C_e/q_m \quad (3)$$

where, q_e (mg/g) is the adsorption capacities of the adsorbents for MB at equilibrium; C_e is the concentration of MB solution after adsorption (mg/L); q_m is the maximum adsorption capacity (mg/g); b is the Langmuir adsorption constant (L/mg), which is related to the free energy of adsorption. K (L/g) and n (dimensionless) are the Freundlich isotherm constant and the heterogeneity factor (a

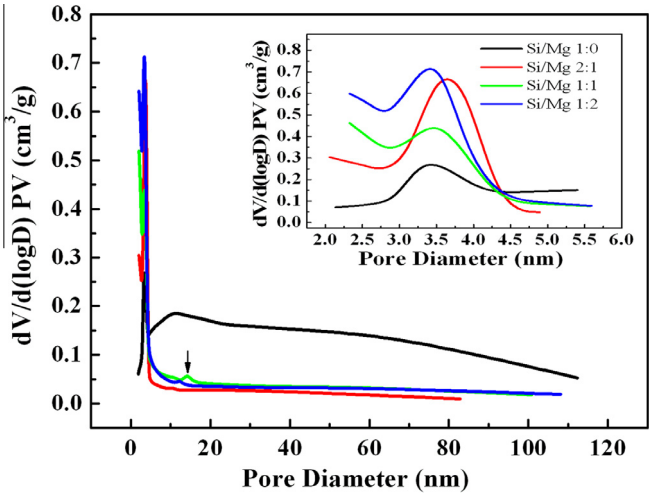

Fig. 6. Pore size distribution curves of modified PAL samples.

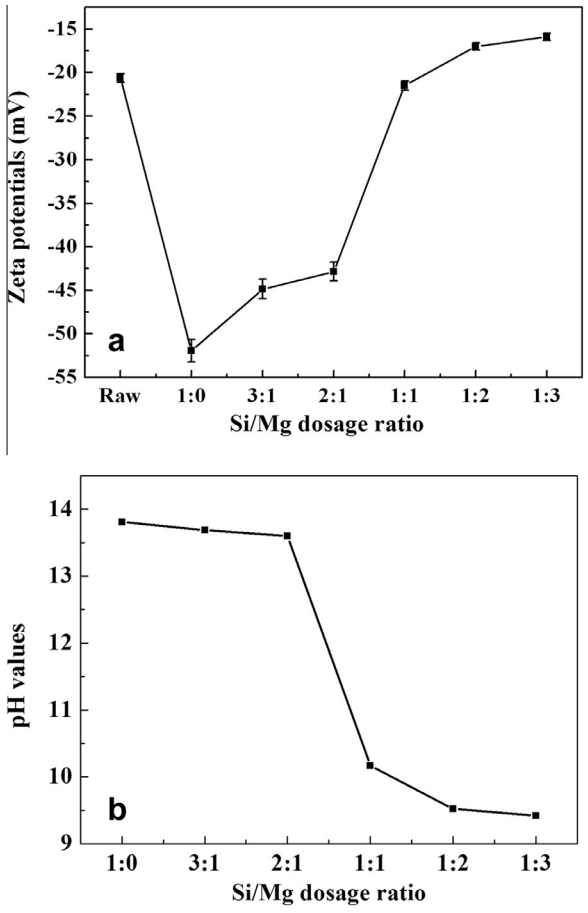

Fig. 7. (a) Variation curves of Zeta potentials with altering the Si/Mg dosage ratio; (b) the pH values of the initial suspension with different Si/Mg dosage ratio.

measure of adsorption intensity or surface heterogeneity), respectively. These parameters can be obtained by fitting the experimental data using the Langmuir (C_e/q_e *vs* C_e) and Freundlich ($\log q_e$ *vs* $\log C_e$) isotherm models (see Table 1). As can be seen, the linear correlation coefficient R^2 is 0.9866 for Langmuir model (Fig. S2, see Supporting materials), and R^2 is larger than 0.9963 for Freundlich isotherm model (Fig. S3, see Supporting materials). This proves that Freundlich isotherm model has a better fitting with adsorption data than the Langmuir isotherm model. The applicability of Freundlich isotherm suggests that different sites with several adsorption energies are involved, and in some cases, the intermolecular interactions occur between dye molecules and PAL.

As shown in Fig. 8, the adsorption of the adsorbents for Cu(II) ions exhibits similar change tendency with that for MB. Compared with raw PAL, the adsorbents show excellent adsorption and removal capability for Cu(II), and the adsorbent with Si/Mg dosage ratio of 2:1 give the maximum adsorption capacity of 210.64 mg/g. As described above, the adsorption data of the adsorbent for Cu(II) was also fitted with Langmuir (Eq. (3)) and Frenderich (Eq. (2)) isotherm modes, and the results are listed in Table 2. It is obvious that the linear correlation coefficients fitted by Langmuir model are larger than 0.99 (Fig. S4, see Supporting materials), and the theoretical q value (213.68 mg/g) is almost equal to the experiment value (210.64 mg/g). However, the fitting result by Frenderich model only has lower R^2 value (0.9731) (Fig. S5, see Supporting materials), and the theoretical q value is far away from the experimental value. This means that the Langmuir isotherm model is suitable to describe the adsorption behavior, and the mono-layer adsorption was suggested. For the adsorption of MB and Cu(II), the $1/n$ value is smaller than 1, which reveals a mono-layer adsorption.

3.8. Adsorption kinetics

Adsorption rate is related to the usage efficiency and is especially important to an adsorbent. As shown in Fig. 9, the adsorption amount of the adsorbents for MB shows a rapid increase with prolonging the contact time, and the adsorption equilibrium can be almost reached within 30 min. For exploring the adsorption mechanism, such as mass transfer and chemical reaction, the pseudo-first-order (Eq. (4)) and pseudo-second-order (Eq. (5)) kinetic equations were used to express the adsorption data [35,36]:

$$\log(q_e - q_t) = \log q_e - (k_1/2.303)t \quad (4)$$

$$t/q_t = 1/k_2 q_e^2 + t/q_e \quad (5)$$

where q_e and q_t are the adsorption capacities of the adsorbents for MB (mg/g) at equilibrium and time t (s), respectively. k_1 is the pseudo-first-order rate constant (s^{-1}), and k_2 is the pseudo-second-order rate constant (mg/g/s). k_1 and k_2 values can be calculated by the slope and intercept from the straight lines of $\log(q_e - q_t)$ *vs* t and t/q_t *vs* t, respectively (Table 3). The initial adsorption rate constant k_{2i} (mg/g/s) is equal to $k_2 q_e^2$ (Table 3). As can be seen, the theoretical q_e values obtained by fitting the experimental data with pseudo-first-order kinetic model are far away from the experimental values, and the linear correlation coefficient is lower than 0.9845 (Fig. S6, see Supporting materials). Whereas the theoretical q_e values obtained by fitting with pseudo-second-order model would be more close to the experimental values, and the correlation coefficient R^2 is larger than 0.9981 (Fig. S7, see Supporting materials). This indicates that the adsorption kinetics could be described by the pseudo-second-order kinetic model very well. Generally, the adsorbates may be transferred from the bulk solution to the adsorbent by a diffusion process. The possibility of the intra-particle diffusion could be evaluated by using the intra-particle diffusion model (Eq. (6)) proposed by Weber and Morris [37]:

$$q_t = k_d * t^{(1/2)} \quad (6)$$

where q_t is the amount of adsorbates adsorbed on the adsorbent at time t, k_d is the intra-particle diffusion rate constant. The plots of q_t *vs* $t^{(1/2)}$ based on the experimental data are shown in Fig. S8 (see Supporting materials). Two distinct regions could be observed: the initial portion of the curve is corresponding to the external surface adsorption (the boundary layer diffusion effects); and the sec-

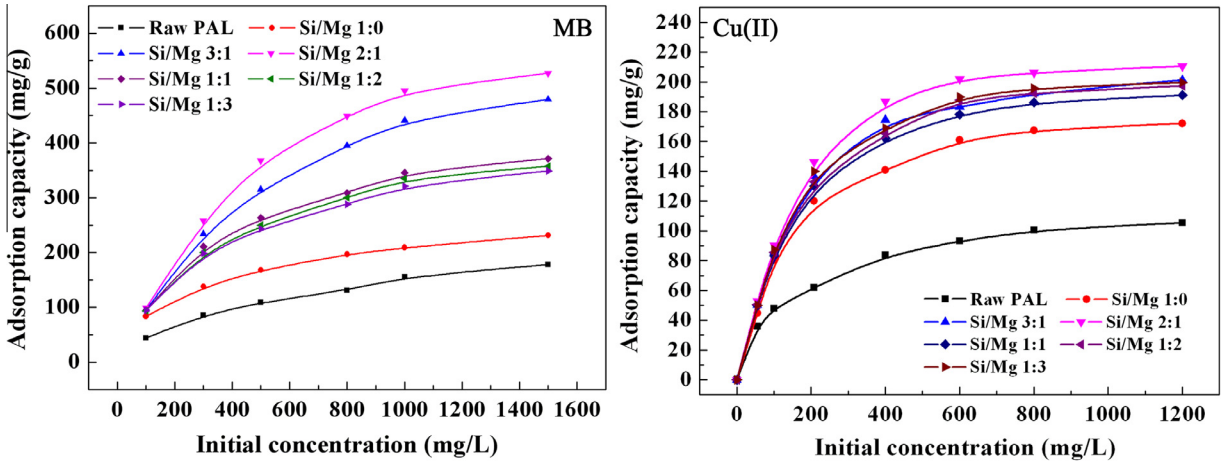

Fig. 8. Effect of initial concentrations on the adsorption capacity of raw PAL and the adsorbents for MB and Cu(II) ion.

Table 1
Adsorption isotherm parameters for the adsorption of MB.

Samples	Langmuir equation			Freundlich equation		
	q_m (mg/g)	b (L/mg)	R^2	K	n	R^2
Raw PAL	212.77	0.0032	0.9866	2.4213	2.2660	0.9986
Si/Mg 1:0	242.72	0.0095	0.9948	5.0998	4.2176	0.9991
Si/Mg 3:1	502.51	0.0140	0.9963	6.0606	3.2959	0.9963
Si/Mg 2:1	543.48	0.0227	0.9977	7.4335	3.9873	0.9972
Si/Mg 1:1	386.10	0.0135	0.9955	6.0057	3.8270	0.9975
Si/Mg 1:2	374.53	0.0126	0.9953	5.9109	3.8491	0.9985
Si/Mg 1:3	362.32	0.0120	0.9936	6.0116	4.0502	0.9987

Table 2
Adsorption isotherm parameters for the adsorption of Cu(II) ions.

Samples	Langmuir equation			Freundlich equation		
	q_m (mg/g)	b (L/mg)	R^2	K	n	R^2
Raw PAL	111.86	0.0120	0.9977	3.3190	3.5750	0.9956
Si/Mg 1:0	177.62	0.0250	0.9993	4.8136	4.1839	0.9684
Si/Mg 3:1	204.50	0.0333	0.9994	5.3762	4.4705	0.9826
Si/Mg 2:1	213.68	0.0505	0.9997	4.9728	3.8187	0.9731
Si/Mg 1:1	195.69	0.0314	0.9995	4.9642	4.0943	0.9799
Si/Mg 1:2	202.02	0.0338	0.9994	5.0008	4.0378	0.9722
Si/Mg 1:3	204.08	0.0370	0.9996	5.0139	4.0014	0.9653

ond less sloping linear portion indicates the gradual adsorption stage leading to the equilibrium (intra-particle diffusion) [38]. This indicates that the overall kinetics of the adsorption process is probably controlled by the surface adsorption and intra-particle diffusion. From Table 3, it can be concluded that the initial adsorption rate of the adsorbents for MB in the solutions with the initial concentration of 200 and 800 mg/L follows the order: Si/Mg 2:1 (800 mg/L) > raw PAL (800 mg/L) > Si/Mg 2:1 (100 mg/L) > raw PAL (100 mg/L), which suggests a faster adsorption rate of the adsorbent than raw PAL. For the same sample, the adsorption rate at higher initial concentration is faster than that at lower initial concentration due to the higher concentration gradient.

Fig. 9 shows the adsorption kinetic curves of the adsorbent for Cu(II) ions. The adsorption kinetic curves exhibit similar change tendency with prolonging the contact time, and adsorption equilibrium was rapidly reached within 30 min. The adsorption kinetic was fitted with the pseudo-first order and pseudo-second-order models and the results are shown in Table 4. It is obvious that the pseudo-second-order kinetic model is more suitable to describe the adsorption process because the R^2 value is higher (>0.9956) (Figs. S9 and S10, see Supporting materials). As shown in Fig. S11, the plots of q_t *vs* $t^{(1/2)}$ for Cu(II) adsorption also show two regions, which reveals that the physical diffusion and interior dispersion contribute to the adsorption process. The adsorption kinetic constants are in the order of Si/Mg 2:1 (200 mg/L) > Si/Mg 2:1 (50 mg/L) > raw PAL (200 mg/L) > raw PAL (50 mg/L). Like the

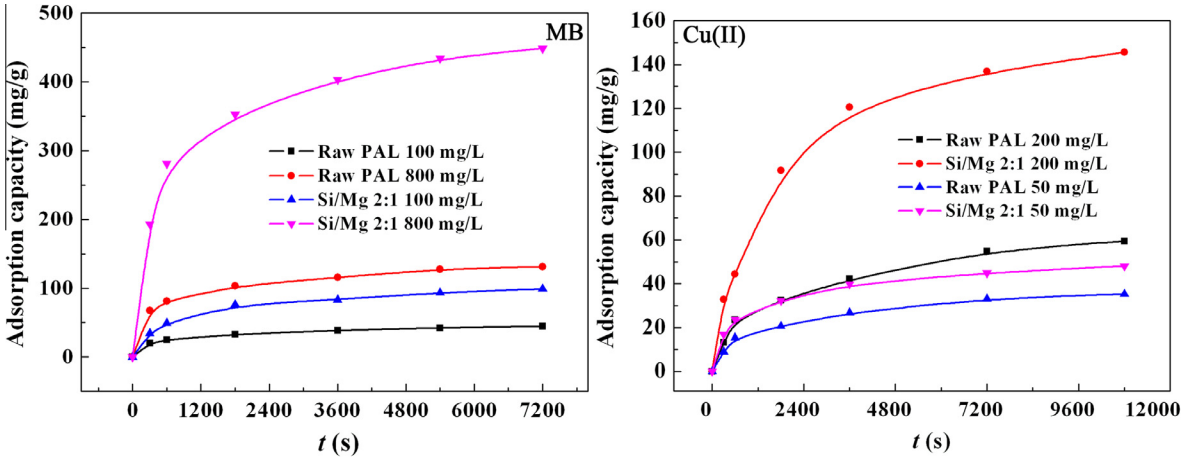

Fig. 9. Influences of contact time on the adsorption capacities of the modified PAL for MB and Cu(II) ions.

Table 3
Adsorption kinetic parameters for the adsorption of MB on raw PAL and the adsorbent.

	Pseudo-first-order model				Pseudo-second-order model			
	$q_{e,exp}$ (mg/g)	$q_{e,cal}$ (mg/g)	$k_1 \times 10^4$ (s^{-1})	R	$q_{e,cal}$ (mg/g)	$k_2 \times 10^5$ (g/(mg s))	k_{2i} (mg/(g s))	R
Raw PAL 100 mg/L	44.46	32.07	5.0414	0.9845	47.24	3.5245	0.0786	0.9981
Raw PAL 800 mg/L	131.25	90.16	5.7716	0.9763	137.93	1.5497	0.2948	0.9986
Si/Mg 2:1 100 mg/L	99.02	75.57	4.8732	0.9802	107.07	1.2547	0.1438	0.9984
Si/Mg 2:1 800 mg/L	448.83	314.51	5.7097	0.9837	476.19	0.4126	0.9355	0.9993

Table 4
Adsorption kinetic parameters for the adsorption of Cu(II) ions on raw PAL and the adsorbent.

	Pseudo-first-order model			Pseudo-second-order model			
	$q_{e,cal}$ (mg/g)	$k_1 \times 10^4$ (s^{-1})	R^2	$q_{e,cal}$ (mg/g)	$k_2 \times 10^5$ (g/(mg s))	k_{2i} (mg/(g s))	R^2
Raw PAL 200 mg/L	51.65	3.3283	0.9911	66.62	0.9892	0.0439	0.9956
Si/Mg 2:1 200 mg/L	124.11	3.8851	0.9910	164.20	0.4375	0.1180	0.9995
Raw PAL 50 mg/L	29.49	3.6050	0.9911	38.84	2.0825	0.0314	0.9985
Si/Mg 2:1 50 mg/L	34.64	3.5301	0.9798	49.97	2.3768	0.0618	0.9989

adsorption behavior for MB, the 2:1 sample also shows the fastest adsorption rate for Cu(II) ions. The diffusion process for Cu(II) adsorption is due to the greater specific surface area of the adsorbents and electrostatic attraction interaction, and the chemical adsorption process is due to the interaction of the functional groups with metal ions. In addition, the Mg^{2+} ion in the adsorbent may exchange with the Cu(II) ions in the solution, which is favorable to the adsorption.

3.9. Effect of external pH values on adsorption

Fig. 10 shows the effects of pH on the adsorption of the adsorbent for MB and Cu(II) ions. It can be noticed that the adsorption capacity for both MB and Cu(II) increased and then tends to be constant. At lower pH value, the surface groups of the adsorbent exist in the form of $–Si–OH_2^+$, and more H_3O^+ ions are existed in the solution. These ions may generate a competition with Cu(II) ions or MB molecules to restrain the adsorption of MB and Cu(II) onto the surface active sites [39,40]. At higher pH, however, the –Si–OH groups tend to transform as $–Si–O^-$ groups, which has relatively stronger electrostatic or chemical association interaction with Cu(II) or MB [16,39], and thus facilitate to the adsorption of positively charged adsorbates onto the negatively charged adsorbent. The evident dependence of adsorption capacity on external pH values gives direct information that the electrostatic interaction is important to the adsorption process. From above analyses, the main influence

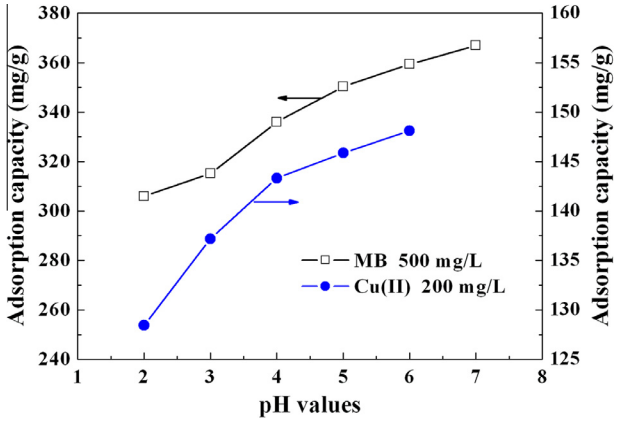

Fig. 10. Effect of external pH values on the adsorption of the adsorbent (Si/Mg dosage ratio, 2:1) for MB and Cu(II).

factors for the adsorption capability of the adsorbent to MB and Cu(II) can be correlated. The adsorption capacity is not highly dependent on the specific surface area, but is clearly affected by the surface charges and state of chemical groups (i.e., $–Si–O^-$). This means that the electrostatic interaction and chemical association of the active groups mainly contribute to the adsorption process.

3.10. Removal efficiency

The adsorbents show excellent removal capability to MB and Cu(II) ion in the solution, which can remove 99.3% of MB (initial concentration, 100 mg/L) and 99.6% of Cu(II) ions (initial concentration, 25 mg/L) from aqueous solution at the adsorbent dosage of 1 g/L, which is clearly higher than that of raw PAL (only 44.1% for MB and 64.3% for Cu(II)). The digital photo gives a more visible indication about the removal of MB and Cu(II) ions (Fig. 11). As can be seen, the deep-blue MB solution (100 mg/L) may almost be completely decolored. For Cu(II), the solution with initial Cu(II)

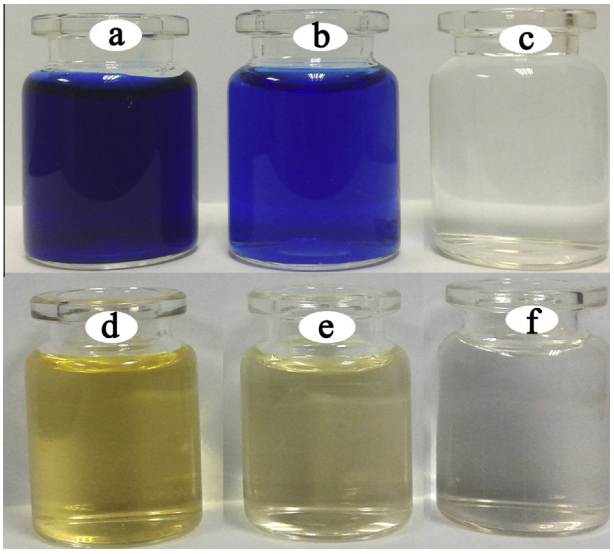

Fig. 11. Digital photos of (a) 100 mg/L MB solution; (b) MB solution after adsorption by raw PAL; (c) MB solution after adsorption by the Si/Mg 2:1 adsorbent; (d) 25 mg/L of Cu(II) solution; (e) Cu(II) solution after adsorbed by raw PAL; (f) Cu(II) solution after adsorbed by the Si/Mg 2:1 adsorbent. For (d–f), the chromogenic reagent of Cu(II) was added to indicate the change of Cu(II) concentration before and after adsorption.

concentration of 25 mg/L shows deep yellow color after adding the chromogenic reagent of Cu(II) Neocuproine Hemihydrate. The color slightly becomes shallow, whereas the solution after adsorption becomes almost colorless even also adding chromogenic reagent. This indicates that the adsorbent is greatly superior to the raw PAL and can be used as efficient and promising adsorbent for the decontamination of wastewater containing cationic dye and Cu(II) ions.

4. Conclusion

In summary, a general one-step hydrothermal route has been developed for the effective preparation of the hybrid adsorbents with excellent adsorption capability to cationic dye and Cu(II). In the reaction process, the structure of PAL was slightly altered and it turns to be more suitable for the adsorption. The magnesium silicate was *in-situ* formed and compounded with PAL to form a new hybrid adsorbent. Intriguingly, the inert quartz associated with PAL mineral may transfer into magnesium silicate with adsorption activity, which provides a new approach for the utilization of quartz-rich PAL minerals. The obtained adsorbents are inclined to be amorphous, and have higher specific surface area (407.3 m^2/g), with more narrow mesopores. The alkaline condition plays an important role for the formation of the adsorbent, and the as-prepared hybrid adsorbents showed an excellent ability to remove cationic dye and heavy metal ions, and are expected to be useful in many other applications. The maximum adsorption capacity of 527.22 mg/g for MB and 210.64 mg/g for Cu(II) ion was obtained at the Si/Mg dosage ratio of 2:1, and it can almost completely remove MB in the 100 mg/L of MB solution and Cu(II) ion in the 25 mg/L of Cu(II) solution. The adsorption isotherm and kinetics suggest that the physical and chemical adsorption contributes to the whole adsorption process, and the electrostatic, ion-exchange and chemical association are responsible for the enhanced adsorption. More importantly, the adsorbents are derived from natural PAL minerals and non-toxic and environment-compatible elements, e.g., Si, Mg, Na, which are new types of low-cost, high-efficient, non-toxic and eco-friendly adsorbents. Therefore, the adsorbent could be regarded as a promising adsorbent for MB dye and Cu(II) removal from water treatment, and can be used as indeed perfect candidates of absorbents for dye and heavy metal ions.

Acknowledgements

The authors would like to thank "863" Project of the Ministry of Science and Technology, P.R. China (No. 2013AA032003), National Natural Science Foundation of China (No. 51403221) and the West Light Foundation of The Chinese Academy of Sciences (The Science Development Talent Teach words [2012] No. 179) for financial support of this research.

Appendix A. Supplementary data

Supplementary data associated with this article can be found, in the online version, at http://dx.doi.org/10.1016/j.cej.2014.11.135.

References

[1] N. Morin-Crini, G. Crini, Environmental applications of water-insoluble β-cyclodextrin–epichlorohydrin polymers, Prog. Polym. Sci. 38 (2013) 344–368.
[2] A.Y. Zahrim, C. Tizaoui, N. Hilal, Coagulation with polymers for nanofiltration pre-treatment of highly concentrated dyes: a review, Desalination 266 (2011) 1–16.
[3] J. Gómez-Pastora, E. Bringas, I. Ortiz, Recent progress and future challenges on the use of high performance magnetic nano-adsorbents in environmental applications, Chem. Eng. J. 256 (2014) 187–204.
[4] W.B. Wang, D.J. Huang, Y.R. Kang, A.Q. Wang, One-step in-situ fabrication of a granular semi-IPN hydrogel based on chitosan and gelatin for fast and efficient adsorption of Cu^{2+} ion, Colloid Surf. B106 (2013) 51–59.
[5] K.Y. Kumar, H.B. Muralidhara, Y.A. Nayaka, J. Balasubramanyam, H. Hanumanthappa, Low-cost synthesis of metal oxide nanoparticles and their application in adsorption of commercial dye and heavy metal ion in aqueous solution, Powder Technol. 246 (2013) 125–136.
[6] K. Thirugnanasambandham, V. Sivakumar, J. Prakash Maran, Application of chitosan as an adsorbent to treat rice mill wastewater—mechanism, modelling and optimization, Carbohydr. Polym. 97 (2013) 451–457.
[7] W.B. Wang, L. Zong, A.Q. Wang, A nanoporous hydrogel based on vinyl-functionalized alginate for efficient absorption and removal of Pb^{2+} ions, Int. J. Biol. Macromol. 62 (2013) 225–231.
[8] S. Barreca, S. Orecchio, A. Pace, The effect of montmorillonite clay in alginate gel beads for polychlorinated biphenyl adsorption: isothermal and kinetic studies, Appl. Clay Sci. 99 (2014) 220–228.
[9] M. Kıranşan, R.D.C. Soltani, A. Hassani, S. Karaca, A. Khataee, Preparation of cetyltrimethylammonium bromide modified montmorillonite nanomaterial for adsorption of a textile dye, J. Taiwan Inst. Chem. Eng. 45 (2014) 2565–2577.
[10] S.S. Ray, M. Bousmina, Biodegradable polymers and their layered silicate nanocomposites: in greening the 21st century materials world, Prog. Mater. Sci. 50 (2005) 962–1079.
[11] I.A. Vasiliadou, D. Papoulis, C.V. Chrysikopoulos, D. Panagiotaras, E. Karakosta, M. Fardisd, G. Papavassiliou, Attachment of Pseudomonas putida onto differently structured kaolinite minerals: a combined ATR-FTIR and ^1H NMR study, Colloids Surf., B: Biointerfaces 84 (2011) 354–359.
[12] Y. Liu, Y. Kang, B. Mu, A. Wang, Attapulgite/bentonite interactions for Methylene blue adsorption characteristics from aqueous solution, Chem. Eng. J. 237 (2014) 403–410.
[13] Y. Deng, Z. Gao, B. Liu, X. Hu, Z. Wei, C. Sun, Selective removal of lead from aqueous solutions by ethylenediamine-modified attapulgite, Chem. Eng. J. 223 (2013) 91–98.
[14] T.H. Chen, H.B. Liu, J.H. Li, D. Chen, D.Y. Chang, D.J. Kong, R.L. Frost, Effect of thermal treatment on adsorption–desorption of ammonia and sulfur dioxide on palygorskite: change of surface acid–alkali properties, Chem. Eng. J. 166 (2011) 1017–1021.
[15] Y. Liu, W.B. Wang, A.Q. Wang, Effect of dry grinding on the microstructure of palygorskite and adsorption efficiency for Methylene blue, Powder Technol. 225 (2012) 124–129.
[16] H. Chen, Y.G. Zhao, A.Q. Wang, Removal of Cu(II) from aqueous solution by adsorption onto acid-activated palygorskite, J. Hazard. Mater. 149 (2007) 346–354.
[17] N. Frini-Srasra, E. Srasra, Acid treatment of south Tunisian palygorskite: removal of Cd(II) from aqueous and phosphoric acid solution, Desalination 250 (2010) 26–34.
[18] X.P. Wu, P. Gao, X.L. Zhang, G.P. Jin, Y.Q. Xu, Y.C. Wu, Synthesis of clay/carbon adsorbent through hydrothermal carbonization of cellulose on palygorskite, Appl. Clay Sci. 95 (2014) 60–66.
[19] H. Chen, J. Zhao, A.G. Zhong, Y.X. Jin, Removal capacity and adsorption mechanism of heat-treated palygorskite clay for Methylene blue, Chem. Eng. J. 174 (2011) 143–150.
[20] A.S. Bhatt, P.L. Sakaria, M. Vasudevan, R.R. Pawar, N. Sudheesh, H.C. Bajaj, H.M. Mody, Adsorption of an anionic dye from aqueous medium by organoclays: equilibrium modeling, kinetic and thermodynamic exploration, RSC Adv. 2 (2012) 8663–8671.
[21] Y.Q. Wang, G.Z. Wang, H.Q. Wang, C.H. Liang, W.P. Cai, L.D. Zhang, Chemical-template synthesis of micro/nanoscale magnesium silicate hollow spheres for waste-water treatment, Chem. Eur. J. 16 (2010) 3497–3503.
[22] Q.Q. Ou, L. Zhou, S.G. Zhao, H.J. Geng, J.J. Hao, Y.Y. Xu, H.L. Chen, X.G. Chen, Self-templated synthesis of bifunctional Fe_3O_4@$MgSiO_3$ magnetic sub-microspheres for toxic metal ions removal, Chem. Eng. J. 180 (2012) 121–127.
[23] B. Öztop, T. Shahwan, Modification of a montmorillonite–illite clay using alkaline hydrothermal treatment and its application for the removal of aqueous Cs^+ ions, J. Colloid Interf. Sci. 295 (2006) 303–309.
[24] V. Gionis, G.H. Kacndes, I.D. Kastritis, G.D. Chryssikos, On the structure of palygorskite by mid- and near-infrared spectroscopy, Am. Mineral. 91 (2006) 1125–1133.
[25] D.C. Golden, J.B. Dixon, H. Shadfan, L.A. Kippenberger, Palygorskite and sepiolite alteration to smectite under alkaline conditions, Clays Clay Miner. 33 (1985) 44–50.
[26] W.F. Bradley, The structural scheme of attapulgite, Am. Mineral. 25 (1940) 405–411.
[27] K.S.W. Sing, D.H. Everett, R.A.W. Haul, L. Moscou, R.A. Pierotti, J. Rouquerol, T. Siemieniewska, Physical and biophysical chemistry division commission on colloid and surface chemistry including catalysis, Pure Appl. Chem. 57 (1985) 603–619.
[28] F. Rouquerol, J. Rouquerol, K. Sing, Adsorption by Powders and Porous Solids: Principles, Methodology and Applications, Academic Press, London, 1999.
[29] A. Bakandritsos, T. Steriotis, D. Petridis, High surface area montmorillonite-carbon composites and derived carbons, Chem. Mater. 16 (2004) 1551–1559.
[30] X.Z. Bu, G.K. Zhang, Y.Y. Gao, Y.Q. Yang, Preparation and photocatalytic properties of visible light responsive N-doped TiO_2/rectorite composites, Microporous Mesoporous Mater. 136 (2010) 132–137.
[31] A. Al-Futaisi, A. Jamrah, R. Al-Hanai, Aspects of cationic dye molecule adsorption to palygorskite, Desalination 214 (2007) 327–342.

[32] E.L. Grabowska, G. Gryglewicz, Adsorption characteristics of congo red on coalbased mesoporous activated carbon, Dyes Pigm. 74 (2007) 34–40.
[33] H.M.F. Freundlich, Über die adsorption in lösungen, Z. Phys. Chem. 57 (1906) 385.
[34] I. Langmuir, The adsorption of gases on plane surfaces of glass, mica and platinum, J. Am. Chem. Soc. 40 (1918) 1361–1403.
[35] W. Rudzinsk, W. Plazinski, Kinetics of solute adsorption at solid/solution interfaces: a theoretical development of the empirical pseudo-first and pseudo-second order kinetic rate equations, based on applying the statistical rate theory of interfacial transport, J. Phys. Chem. B 110 (2006) 16514–16525.
[36] Y.-S. Ho, Review of second-order models for adsorption systems, J. Hazard. Mater. B136 (2006) 681–689.
[37] W.J. Weber, J.C. Morris, Kinetics of adsorption on carbon from solution, J. San. Eng. Div. ASCE 89 (1963) 31–59.
[38] R. Qadeer, A study of the factors affecting the adsorption of cobalt ions onto Pakistani coal powder from solutions, J. Radioanal. Nucl. Chem. 295 (2013) 2021–2028.
[39] X.Z. Bu, G.K. Zhang, Y.D. Guo, Thermal modified palygorskite: preparation, characterization, and application for cationic dye-containing wastewater purification, Desalin. Water Treat. 30 (2011) 339–347.
[40] J.H. Potgieter, S.S. Potgieter-Vermaak, P.D. Kalibantonga, Heavy metals removal from solution by palygorskite clay, Miner. Eng. 19 (2006) 463–470.